Published in final edited form as:
J Biol Chem. 2007 November 30; 282(48): 34611–34622. doi:10.1074/jbc.M707795200.

Genetic Ablation of Calcium-independent Phospholipase $A_2\gamma$ Leads to Alterations in Mitochondrial Lipid Metabolism and Function Resulting in a Deficient Mitochondrial Bioenergetic Phenotype*

David J. Mancuso[‡,§], **Harold F. Sims**[‡,§], **Xianlin Han**[‡,§], **Christopher M. Jenkins**[‡,§], **Shao Ping Guan**[‡,§], **Kui Yang**[‡,§], **Sung Ho Moon**[‡,§], **Terri Pietka**[¶,§], **Nada A. Abumrad**[¶,§,||], **Paul H. Schlesinger**[||], and **Richard W. Gross**[‡,§,**,‡‡,1]

[‡] Division of Bioorganic Chemistry and Molecular Pharmacology, Washington University School of Medicine, St. Louis, Missouri 63110

[¶] Division of Nutritional Sciences, Washington University School of Medicine, St. Louis, Missouri 63110

[§] Department of Medicine, Washington University School of Medicine, St. Louis, Missouri 63110

[||] Department of Cell Biology and Physiology, Washington University School of Medicine, St. Louis, Missouri 63110

[**] Department of Molecular Biology and Pharmacology, Washington University School of Medicine, St. Louis, Missouri 63110

[‡‡] Department of Chemistry, Washington University, St. Louis, Missouri 63130

Abstract

Previously, we identified a novel calcium-independent phospholipase, designated calcium-independent phospholipase A_2 γ (iPLA$_2\gamma$), which possesses dual mitochondrial and peroxisomal subcellular localization signals. To identify the roles of iPLA$_2\gamma$ in cellular bioenergetics, we generated mice null for the iPLA$_2\gamma$ gene by eliminating the active site of the enzyme through homologous recombination. Mice null for iPLA$_2\gamma$ display multiple bioenergetic dysfunctional phenotypes, including 1) growth retardation, 2) cold intolerance, 3) reduced exercise endurance, 4) greatly increased mortality from cardiac stress after transverse aortic constriction, 5) abnormal mitochondrial function with a 65% decrease in ascorbate-induced Complex IV-mediated oxygen consumption, and 6) a reduction in myocardial cardiolipin content accompanied by an altered cardiolipin molecular species composition. We conclude that iPLA$_2\gamma$ is essential for maintaining efficient bioenergetic mitochondrial function through tailoring mitochondrial membrane lipid metabolism and composition.

Mitochondria transduce chemical energy from multiple dietary substrates into ATP and heat and are important participants in cellular lipid metabolism and signaling (1,2). Through the precisely regulated partitioning of energy derived from substrates between ATP synthesis and

*This research was supported by National Institutes of Health Grant 5PO1HL57278-10 and by Clinical Nutrition Research Unit Grant DK56351.

[1]To whom correspondence should be addressed: Washington University School of Medicine, Division of Bioorganic Chemistry and Molecular Pharmacology, 660 S. Euclid Ave., Campus Box 8020, St. Louis, MO 63110. Tel.: 314-362-2690; Fax: 314-362-1402; rgross@wustl.edu.

heat production, a finely tuned dynamic balance is maintained to promote organism survival. In addition, excess energy derived from substrates, not immediately needed to fulfill chemical or thermodynamic demands, is directed into the production of lipid synthetic intermediates for energy storage (*e.g.* mitochondrial synthesis of lysophosphatidic acid, a precursor of triglycerides). Moreover, mitochondria generate diverse chemical signals that reflect the bioenergetic status of the cell (*e.g.* NO and cytochrome *c*) and thus integrate multiple energetic, metabolic, and signaling cascades (1–5).

Mitochondrial phospholipases are important participants in the regulation of mitochondrial function and signaling (6–11). Mitochondrial phospholipases catalyze the production of non-esterified fatty acids that regulate UCP function, release lipid second messengers, such as 2-arachidonoyl lysophosphatidylcholine (LPC),[2] and modulate membrane molecular dynamics (12). Maladaptive activation of phospholipases has deleterious metabolic effects in many systems, and previous studies have implicated calcium-independent phospholipases A_2 ($iPLA_2$s) as the enzymic mediators of membrane dysfunction in diabetic cardiomyopathy (13–16). Metabolic flexibility is dependent on the efficient coordinated transitions of substrate flux that occur during alterations in energy sources (*e.g.* glucose *versus* fatty acid) or energy demand (*e.g.* exercise). Obesity and type II diabetes are thought to result from disruption of these transitions (17). Diabetic cardiomyopathy is characterized by altered lipid metabolism (*i.e.* greatly increased utilization of fatty acids) that results in changes in the chemical composition of cardiac membranes, modifying their biophysical properties and function (13, 18–20). Many of the metabolites used in mitochondrial energy metabolism possess dual roles in modulating signaling cascades (*e.g.* acyl-CoA, acylcarnitines, fatty acids, and lysophosphatidic acid), thereby integrating lipid energy metabolism and cellular signaling functions (21–25). Ultimately, the disproportionate utilization of fatty acids in diabetic myocardium leads to a profound metabolic imbalance resulting in bioenergetic inefficiency, resulting, at least in part, from alterations of cardiolipin (CL) molecular species that occur in diabetic myocardium (18,20,26,27).

Previously, we cloned and characterized $iPLA_2\gamma$, a major phospholipase activity in murine myocardium based on activity assays, mRNA content, and kinetic analyses using enantiomeric selective mechanism-based inhibitors (28). Subsequently, $iPLA_2\gamma$ was found to possess dual mitochondrial and peroxisomal localization signals, suggesting its importance in regulating myocardial bioenergetics and lipid metabolism. Next, we demonstrated that cardiac myocyte-specific overexpression of $iPLA_2\gamma$ results in dramatic reductions of cardiac phospholipid mass and mitochondrial dysfunction (29). Remarkably, fasting of cardiac myocyte-restricted $iPLA_2\gamma$ overexpressing mice resulted in large increases in myocardial triglyceride content that precipitated hemodynamic dysfunction (29).

To gain further insight into the role of $iPLA_2\gamma$ in cardiac function, we inactivated the $iPLA_2\gamma$ gene in mice by targeted deletion of exon 5 encoding the lipase active site (GVSTG). Genetic ablation of $iPLA_2\gamma$ resulted in growth retardation, cold intolerance, and dramatically reduced exercise endurance. The importance of $iPLA_2\gamma$ in the ability of myocardium to respond to stress was identified by the dramatically reduced survival of $iPLA_2\gamma$ knock-out mice following transverse aortic constriction. Finally, mitochondrial function assays in mice null for $iPLA_2\gamma$ demonstrated markedly decreased complex IV function that was associated with decreases in tetra-18:2 cardiolipin content. Collectively, these studies identify mitochondrial dysfunction

[2]The abbreviations used are: LPC, Lysophosphatidylcholine; $iPLA_2$, calcium-independent phospholipase A_2; $iPLA_2\gamma$, calcium-independent phospholipase $A_2\gamma$ (AF263613); KO, knock-out; BEL, (*E*)-6-(bromomethylene)-3-(1-naphthalenyl)-2H-tetrahydropyran-2-one; TAC, transverse aortic constriction; CL, cardiolipin; $cPLA_2$, cytosolic phospholipase A_2; WT, wild type; WAT, white adipose tissue; BAT, brown adipose tissue; UCP, uncoupling protein; nt, nucleotide; TMPD, tetramethyl p-phenylene diamine.

resulting from alterations in mitochondrial lipid metabolism as the mechanistic basis for the phenotypic features of mice null for iPLA$_2\gamma$.

EXPERIMENTAL PROCEDURES

Materials

Radiolabeled nucleotides and 1-palmitoyl-2-[1-^{14}C]arachidonoyl phosphatidylcholine were purchased from PerkinElmer Life Sciences. ECL reagents were purchased from GE Life Sciences. PCR reagents were purchased from Applied Biosystems (Foster City, CA) and used with an ABI GeneAmp PCR System 9700 thermocycler. Racemic BEL was purchased from Calbiochem. A rabbit antibody to a peptide derived from the human iPLA$_2\gamma$ sequence was used in these studies and prepared by affinity chromatography as previously described in detail (28). Normal rabbit serum was affinity-purified in an identical manner for use as a control primary antibody. Synthetic phospholipids used as internal standards in mass spectrometric analyses were purchased from Avanti Polar Lipids (Alabaster, AL), Nu-Chek Prep, Inc. (Elysian, MN), and Cambridge Isotope Laboratories, Inc. (Cambridge, MA) and used as described previously (30). Solvents for sample preparation and for mass spectrometric analysis were purchased from Burdick and Jackson (Honeywell International Inc., Burdick and Jackson, Muskegon, MI). Most other reagents were obtained from Sigma.

Ablation of the Active Site of iPLA$_2\gamma$

Mouse genomic DNA was utilized as a template for PCR amplification with primers P1 and P2 (Table 1) to generate a 4917-nt fragment containing sequence 5′ of exon 5 and flanked by EcoRI restriction sites. This fragment was cloned into the corresponding site of vector pPNT (31) upstream of the neomycin gene sequence. Similarly, a 1055-nt PCR fragment amplified utilizing primers P3 and P4 (Table 1) and corresponding to sequence 3′ of exon 6 was cloned into XhoI and NotI restriction sites downstream of the neomycin gene sequence. This generated a construct containing iPLA$_2\gamma$ genomic sequence, for which exon 5 was replaced with the positive selection marker (neomycin in the opposite orientation) and leaving regions of homology on either side of the neomycin gene. An SfiI restriction site within the plasmid construct containing the iPLA$_2\gamma$ was used for linearization. The linearized construct was electroporated into male SCC#10 ES cells (derived from 129X1Sv/J mice; Jackson Laboratories (Bar Harbor, ME)) for subsequent neomycin selection using G418. Homologous recombinants were identified by Southern blot analysis and tail PCR. For genomic Southern blot analysis, PstI restriction site differences between wild type (WT) and KO mouse genomic DNA sequence were utilized for detection of 7.4-kb WT and 5.9-kb KO iPLA$_2\gamma$ bands by hybridization with a 459-nt genomic probe generated by PCR amplification with primers P5 and P6 (Table 1). Two clones of 238 screened by Southern analysis were positive for the homologous recombination. These clones were injected into C57BL/6 blastocysts, followed by implantation into pseudopregnant mice to generate the chimeric mouse founder line utilizing the Neurosciences Transgenic Core facility at Washington University. Chimeras were mated to C57BL6/J mice, and germ line transmission to heterozygous offspring was confirmed by Southern blotting of tail DNA. Interbreeding of heterozygous offspring was used to generate homozygous KO and WT littermates used in all studies. In addition to genomic Southern analysis, tail PCR was routinely performed for genotyping. “Neoforward” and “Common REV” primers (Table 1) were utilized for amplification of a 354-nt product from the knock-out allele, whereas paired “iPLA$_2$ FOR” and “Common REV” primers (Table 1) were utilized to amplify a 181-nt product for detection of the wild type allele. All experiments were performed using sex- and age-matched littermate controls as noted.

General Animal Studies

Animal protocols were in strict accordance with the National Institutes of Health guidelines for humane treatment of animals and were reviewed and approved by the Animal Care Committee of Washington University. Conscious animals fed *ad libitum* were weighed at various time points after weaning up to 10 months of age. Following euthanasia, tissues were dissected from male and female mice, weighed, and expressed as a fraction of total body weight. Rectal temperature was measured to the nearest 0.1°C by inserting the probe of a thermocouple (Fisher) 20 mm into the rectum until a stable reading was obtained. For these temperature studies, mice were singly housed at ambient temperature with food and water provided *ad libitum*, and the mean of temperatures taken at 8 a.m. on three consecutive days was reported. For cold tolerance studies, male and female WT and KO mice were singly housed at 4°C for up to 24 h with food and water provided *ad libitum*. For cold adaptation studies, core body temperatures were monitored utilizing a rectal probe at time 0 and hourly thereafter with constant monitoring of mice for signs of lethargy. Mice were removed from the study when their core temperature dropped below 28°C. For food intake studies, *ad libitum* food intake of individually housed mice was measured at 1, 1.5, 4, and 9 months of age ($n = 4$) over a period of 3–5 consecutive days.

RNA, DNA, and Protein Analyses

For Northern blotting, total RNA was isolated utilizing an RNeasy tissue kit, and hybridizations were performed as previously described (8), utilizing labeled ~1-kb iPLA$_2\gamma$ probe derived from IMAGE clone 6591346 (ATCC, Manassas, VA). For quantitative PCR analyses, total RNA was isolated from tissues using Trizol (Invitrogen) according to the manufacturer's directions. RNA was quantified by spectrophotometry (NanoDrop, Wilmington, DE). cDNA was synthesized from RNA using Superscript III Reverse Transcriptase (Invitrogen). cDNA samples were amplified using Power SYBR Green PCR Master Mix (Applied Biosystems) on the ABI 7500 real time PCR system (Applied Biosystems). Acidic ribosomal protein 36B4 message was used for normalization, and results were analyzed using the comparative *Ct* method. Primers used for quantitative PCR were as follows (5′ –3′): UCP1, CTCACTCAGGATTGGCCTCTA (forward) and TCTGACCTTCACGACCTCTGTA (reverse); UCP2, TCCACGCAGCCTCTACAAT (forward) and GACCTTTACCACATCTGTAGGC (reverse); UCP3, CAGAGGGACTATGGATGCCTAC (forward) and AGGTGAGACTCCA-GCAACTTCT (reverse); 36B4, GCAGACAACGTGGGCTCCAAGCAGAT (forward) and GGTCCTCCTTGGTGAACACGAAGCCC (reverse). Results were analyzed by comparing the threshold crossing (*Ct*) of each sample after normalization to the control genes (*dCt*). The changes in the threshold crossing (*dCt*) were used to calculate the relative levels of each mRNA from the various samples using the formula 2^{-dCt}. Genomic Southern blot studies were performed by PstI digestion of 10 mg of genomic DNA, followed by electrophoreses on a 0.8% TAE gel and transfer to a Hybond-XL (GE Life Sciences) membrane for hybridization. Western blotting was performed as previously described (28) utilizing an ECL detection system (GE Life Sciences).

Treadmill Studies

Treadmill studies were performed utilizing the Mouse Cardiovascular Phenotyping Core at Washington University School of Medicine. WT and knock-out mice (ages ~2–9 months) were run to exhaustion utilizing a motorized, speed-controlled, modular treadmill system (Columbus Instruments, Columbus, OH) equipped with an electric shock stimulus and an adjustable inclination angle as previously described (32). Runs were performed on a level inclination, and running velocity was initiated at 10 m/min and then incrementally increased at a rate of 3 m/min until exhaustion, defined as the inability to remain on the treadmill for 5 s.

Transverse Aortic Constriction

Transverse Aortic Constriction studies were performed by the Mouse Cardiovascular Phenotyping Core at the Washington University School of Medicine. The protocol for transverse aortic constriction (TAC) has been previously described (33,34). In brief, surgery was performed on mice anesthetized with a xylazine (16 mg/kg) and ketamine (80 mg/kg) mixture, and a 7–0 silk suture was placed around the transverse aorta and tied around a 25-gauge blunt needle, which was subsequently removed. Following constriction, the gradient across the band was measured to ensure that adequate stenosis had been achieved. Subsequently, the thorax was closed, and mice were allowed to recover on a heating pad until responsive to stimuli. Surgeons were blinded to mouse genotypes. As controls, sham-operated animals underwent identical surgery but without aortic constriction.

Mitochondrial Respiration Studies

Mitochondria were prepared essentially as previously described (35,36). Hearts were removed from WT and knock-out animals and immediately placed at 10% (w/v) into ice-cold pH 7 HEPES buffer containing 1 mM EDTA and 250 mM sucrose. Hearts were homogenized with a loose fitting dounce homogenizer. Next, the homogenate was centrifuged at 500 × *g* for 10 min to remove cellular debris, nuclei, and connective tissue. The supernatant solution was centrifuged at 9,000 × *g* for 35 min to isolate mitochondria, which were resuspended in homogenization buffer. Protein concentration was determined using the micro-BCA protein assay kit (Pierce). Oxygen consumption was measured polarographically using a dual channel Instech dissolved oxygen measuring system. In the presence of malate and succinate, O_2 consumption was initiated with ADP to determine substrate-supported O_2 consumption and ability to generate ATP. Cytochrome oxidase activity, after the addition of rotenone, was determined by the addition of ascorbate and TMPD. The addition of azide completely abolished oxygen uptake in the rote-none-inhibited preparation.

Mass Spectrometric Analysis of CL

Enhanced shotgun lipidomics analyses of CL were performed on a QqQ mass spectrometer (Thermo-Fisher Scientific, San Jose, CA) equipped with an electrospray ion source as previously described (26). All electrospray ionization mass spectrometric analyses of lipids were conducted by direct infusion employing a Harvard syringe pump at a flow rate of 4 μl/min. Typically, a 1-min period of signal averaging was employed for each mass spectrum, and a 2-min period of signal averaging was employed for each tandem mass spectrometric spectrum. A mass resolution of 0.4 Thomson was employed for acquisition of mass spectra with a QqQ instrument.

Statistical Analysis

Data were analyzed using a two-tailed Student's *t* test, χ test, one-way analysis of variance (for treadmill studies), and the log-rank test (for TAC studies). Differences were regarded as significant at $p < 0.05$. All data are reported as the mean ± S.E. unless otherwise noted.

RESULTS

Targeted Disruption of the iPLA$_2\gamma$ Gene

Since iPLA$_2\gamma$ has multiple promoters and splice variants (8,28), we employed a knock-out strategy targeting the ablation of exon 5, which contains the active site. A neomycin-based gene-targeting vector was designed to undergo homologous recombination, leading to deletion of exon 5 of the murine iPLA$_2\gamma$ gene. The strategy for the targeting event employed to effect homologous recombination and the multiple methods used for its identification are shown in Fig. 1*A*. First, a linearized vector was used to electroporate SCC#10 ES cells (derived from

129X1/SvJ mice) as described under "Experimental Procedures." After neomycin selection, colonies were screened for targeted disruption of exon 5 by Southern blot analyses. Of the 238 ES clones identified possessing the neomycin resistance cassette, two independent clones (clones 7 and 48) exhibited evidence of the desired insertion/recombination event. These clones were separately injected into C57BL/6 blastocysts and implanted into pseudopregnant females as described under "Experimental Procedures." Male chimeras (10 chimerics from clone 7 and 1 chimeric from clone 48) whose coat color ranged from 50 to 100% agouti were subsequently bred with C57BL/6 mice. Heterozygotes originating from clone 7 were used for the subsequent generation of all mice. Breeding of C57BL/6 mice containing the insert from clone 7 led to the generation of viable mice null for the iPLA$_2\gamma$ gene as demonstrated by both tail PCR analyses and genomic Southern analyses (Fig. 1*B*).

Further characterization of the targeting strategy for the disruption of the iPLA$_2\gamma$ gene demonstrated that the ablation of exon 5 resulted in an unstable transcript, since multiple different regions of the gene could not be detected by reverse transcription-PCR analyses (Fig. 1*C*) and Northern blot analyses of

mRNA purified from heart and other tissues in iPLA$_2\gamma$ KO mice did not demonstrate any message corresponding to the altered transcript (Fig. 1*D*). Targeted disruption of the iPLA$_2\gamma$ active site resulted in over a 60% reduction in the production of 2-[^{14}C]arachidonoyl LPC from 1- palmitoyl 2-[^{14}C]arachidonoyl-PC in incubations with mitochondrial homogenates prepared from mice null for iPLA$_2\gamma$ (Fig. 2). The marked reduction in this "signature" reaction of iPLA$_2\gamma$ substantiates the targeted ablation of iPLA$_2\gamma$ activity. The remaining measurable mitochondrial phospholipase activity was probably largely due to iPLA$_2\beta$, since it was inhibitable by BEL, and substantive amounts of iPLA$_2\beta$ are known to be present in murine mitochondria (7,9). In addition, iPLA$_2\beta$ can hydrolyze the *sn*-1-position of 1-palmitoyl-2-arachidonoyl choline glycerophospholipids, albeit at much slower rates and with less regiospecificity in comparison with iPLA$_2\gamma$ (12). It should be noted that small amounts of a calcium-independent activity that was not inhibitable by BEL were also present in both WT and iPLA$_2\gamma^{-/-}$ murine mitochondria. This activity probably results from cPLA$_2\gamma$ that is localized in the mitochondrial compartment and is both calcium-independent and not inhibitable by BEL (37). Taken together, these results support the conclusion that the gene-targeting event resulted in an iPLA$_2\gamma$ null allele and that iPLA$_2\gamma^{-/-}$ mice were viable.

General Phenotypic Features of Mice Null for iPLA$_2\gamma$

Subsequent large scale breeding of heterozygous mice resulted in normal litter sizes with no unexpected deaths of offspring. Genotypic analyses of 751 offspring from heterozygous crosses resulted in 201 WT, 395 heterozygous, and 155 homozygous KO offspring, indicating a small (17%) reduction in the expected Mendelian inheritance of the homozygous KO (0.89: 2.26:1.15 *versus* the expected 1:2:1 ratio ($p < 0.02$ by the χ test). Most of the reduction was due to the lower proportion of female KO mice (71 *versus* the expected 94), a 24% reduction in anticipated female offspring ($p < 0.05$). Although iPLA$_2\gamma$ knock-out mice appeared normal and healthy after birth and weaning by visual inspection, body weights of iPLA$_2\gamma$ KO mice were consistently 9% lower compared with sex-matched WT littermates (8.78 ± 0.4 *versus* 10.95 ± 0.2 g, respectively, at 28 days of age ($p < 0.01$)) and remained lower through approximately day 50 (Fig. 3*A*). In contrast to their WT littermates, which progressively increased in weight, mice null for iPLA$_2\gamma$ did not gain significant weight after adolescence. By day 288, KO male animals had a mean weight of 22.2 ± 0.4 g *versus* 34.1 ± 3.1 g for WT males (*i.e.* 35% lower weight). Female KO animals weighed 21.4 ± 1.1 *versus* 31.2 ± 5.2 g for WT females at day 255 (31% lower weight) (Fig. 3*B*). Along with a reduction in body mass, by 9 months of age, KO male mice had a significantly shorter body length by ~8% (measured from the tip of the nose to the anus). KO mice were 9.3 ± 0.1 cm *versus* 10.0 ± 0.1 cm for WT

littermates ($p < 0.001$, $n = 11$ WT and 13 KO). A slightly reduced food intake (9%) was identified for the 2–3-month-old iPLA$_{2}\gamma$ KO animals, which was not statistically significant. In contrast, a 24% reduction in food intake was observed in 9-month-old male KO animals (3.7 g/day for KO *versus* 4.7 g/day for WT, $p < 0.06$, five separate measurements of $n = 6$ per group). This reduction was not significant after adjusting for differences in body weight. Both male and female KOs (between 3 and 12 months of age) had a significantly lower basal core body temperature by nearly 0.5°C. The mean core body temperatures were 36.3 ± 0.1°C (WT males) *versus* 35.7 ± 0.1°C (KO males, $p < 0.02$) and 36.8 ± 0.1°C (WT females) *versus* 36.4 ± 0.1°C (KO females) based on n of ~19 per genotype and an average of 50 readings per genotype. The weights of brain, liver, kidney, skeletal muscle, brain, WAT, and BAT relative to total body weight were not significantly different compared with wild type littermates. Other measured parameters, including fasting blood glucose levels (116.5 ± 11.3 mg/dl; average blood pressure measured by five consecutive tail cuff readings (99.4 ± 8.16/86.2 ± 5.7 mm Hg for iPLA$_{2}\gamma$ knockout mice *versus* 113.4 ± 1.97/96.9 ± 3.1 mm Hg for wild type littermates)) and glucose tolerance (blood glucose measurements following 16 h of fasting and intraperitoneal glucose administration), were within the normal range and were not significantly different in 2–4-month-old KO and WT littermates. Echocardiographic analyses of iPLA$_{2}\gamma$ mice at ages of 2–3 months did not reveal any significant differences in chamber sizes or ventricular function compared with WT control mice fed *ad libitum*, after fasting, or after high fat feeding for 6 weeks. No differences were found between iPLA$_{2}\gamma$ knock-out mice and iPLA$_{2}\gamma$ controls in general ambulatory activity studies (data not shown).

Compromised Thermal Adaptation in iPLA$_{2}\gamma$ KO Mice

To compare the ability of 4–6-month-old WT and iPLA$_{2}\gamma$ KO animals to adapt to cold, decreases in core body temperature were examined as a function of time following exposure to 4°C with ready access to food and water as described under “Experimental Procedures.” All WT littermates were able to maintain core body temperatures for 24 h at 4°C. In sharp contrast, cold intolerance was manifest in both male and female mice null for iPLA$_{2}\gamma$ (15.3 ± 2.7 and 11.5 ± 3.4 h mean endurance times at 4°C, respectively) (Fig. 4). Similarly, aged mice (9–11 months) null for iPLA$_{2}\gamma$ also demonstrated cold intolerance, whereas their WT littermates did not. The mean endurance times for KO male and female animals were 8 ± 0.4 and 7.1 ± 0.6 h, respectively, whereas both WT male and female animals maintained their body temperatures throughout the entire experimental interval. Collectively, these results demonstrated that both young and old iPLA$_{2}\gamma$ knock-out mice had defects in cold adaptation.

Uncoupling of electron transport and conversion of the proton-motive force across the inner membrane into heat by uncoupling proteins (UCPs) is a well described mechanism for heat production. In particular, mitochondrial uncoupling in brown adipose tissue mediated by UCP1 has been previously shown to support body temperature after exposure to cold (reviewed in Ref. 38). Accordingly, we examined levels of mRNA encoding UCP1 levels in brown adipose tissue by reverse transcription-PCR during normothermic and hypothermic conditions (Fig. 5*A*). Although the basal UCP1 message level of the KO is slightly higher than that of WT mice (1.5-fold), the data indicate that both WT and KO mice responded to cold with similar (~2-fold) increases in brown adipose UCP1 mRNA expression after exposure to cold. We also measured levels of UCP2 and UCP3 in cardiac muscle in both WT and KO animals. Although no alterations in UCP2 levels were detected (Fig. 5*B*), iPLA$_{2}\gamma$ KO mice had 8-fold lower levels of UCP3 mRNA as determined by reverse transcription-PCR in comparison with their WT counterparts (Fig. 5*C*).

Decreased Exercise Endurance of iPLA$_{2}\gamma$ KO Mice

Considering the defects in cold adaptation in the iPLA$_{2}\gamma$ KO mice, we next focused on the ability of these mice to tolerate prolonged exercise on a treadmill in comparison with their WT

counter-parts. Interestingly, 53-day-old mice null for iPLA$_2\gamma$ exhibited a dramatic 50% decrease in exercise endurance (19.1 ± 1.3 min) compared with their WT littermates (39.3 ± 1.5 min, $p < 0.001$) when the animals were run to exhaustion on a treadmill (Fig. 6*A*). This exercise deficit was progressive, since the endurance time of 86-day-old KO mice relative to WT decreased to less than 25% relative to WT littermates (9.6 ± 0.7 *versus* 32 ± 3.2 min for the KO *versus* WT, respectively, $p < 0.001$) (Fig. 6*B*). By day 270, the KO treadmill time had further decreased to 5 min (5.3 ± 0.7 min) (Fig. 6*B*).

Compromised Myocardial Functional Reserve in iPLA$_2\gamma$ KO Mice

TAC with careful monitoring of pressure gradients has been a useful model in the evaluation of myocardial metabolic reserve in response to hemodynamic stress. Mice null for iPLA$_2\gamma$ were dramatically more susceptible to sudden death following transverse aortic constriction. Six of 8 knock-out mice (ages 2–4 months) died within 24 h following surgery (25% survival), whereas all of the sham operated mice or wild type littermates survived. No significant alterations in pressure gradients generated by banding between the two groups were present. These results demonstrate that iPLA$_2\gamma$ KO mice are unable to successfully compensate for the increased myocardial energy demands generated by hemodynamic-induced increases in ventricular afterload.

Decreased Mitochondrial Function in iPLA$_2\gamma$ KO Mice Due to Inefficient Complex IV-mediated O_2 Reduction

The markedly decreased survival of mice null for iPLA$_2\gamma$ in response to pressure overload suggested an iPLA$_2\gamma$-induced defect in cardiac mitochondrial function. To determine if this contributed to the increased TAC mortality rate and decreased exercise endurance observed in iPLA$_2\gamma$ knock-out mice, mitochondria were isolated from WT and iPLA$_2\gamma$ KO myocardium for measurement of respiratory function as described under "Experimental Procedures." Initially, the ability of WT and iPLA$_2\gamma$ KO mitochondria to support cytochrome oxidase (Complex IV)-mediated reduction of molecular oxygen in the presence of a surrogate electron donor (ascorbate) was measured. Remarkably, the rate of O_2 consumption by iPLA$_2\gamma$ KO mitochondria was decreased by 65% compared with that of WT controls (Fig. 7*A*). To demonstrate the functional integrity of the isolated mitochondria, ADP, succinate, and malate were added in separate experiments to the mitochondria, which resulted in robust O_2 consumption in both WT and iPLA$_2\gamma$ KO mitochondria with only minimal differences in the rate of O_2 reduction (Fig. 7*B*). After correction for azide inhibition, a replot of ascorbate-TMPD oxygen consumption (relative site IV V_{max}) more dramatically demonstrated the reduced functional activity of complex IV in both young and old iPLA$_2\gamma$ KOs *versus* WT controls (Fig. 7*C*).

Alterations in Cardiolipin Content and Molecular Species Distribution in iPLA$_2\gamma$ KO Mice

To determine if genetic ablation of iPLA$_2\gamma$ resulted in changes in myocardial lipid composition, shotgun lipidomics was performed on heart tissue from WT and KO animals aged 4–6 months. No statistically different alterations in major lipid classes (*e.g.* phosphatidylcholine, phosphatidylethanolamine, phosphatidylglycerol, triacylglycerol, etc.) or molecular species examined were noted with the exception of a decrease in CL content and an altered CL molecular species distribution (Fig. 8). Specifically, the total CL content was reduced by 15 ± 0.2 mol % in iPLA$_2\gamma$ KO hearts in comparison with their wild type littermates (Fig. 9*A*). Moreover, a more marked decrease in the symmetric CL species tetra-18:2 CL was present in mice null for iPLA$_2\gamma$ in comparison with their WT littermates (33 ± 0.6 mol %, $p < 0.02$) (Fig. 9*B*). Similar results were obtained from analyses of hearts from animals 9 –11 months of age (data not shown). The peak at *m*/*z* 747.5 was composed of tri-18:2–22:6 CL and was not substantially changed in WT *versus* iPLA$_2\gamma$ KO mice. Collectively, these results demonstrate

that iPLA$_2\gamma$ participates in mitochondrial cardiolipin metabolism, presumably by supplying the lysocardiolipin acceptor substrate for acylation/transacylation remodeling reactions. Thus, although iPLA$_2\gamma$ is not obligatory for the production of tetra-18:2 CL (*i.e.* tetra-18:2 CL is present in the iPLA$_2\gamma$ KO), the absence of iPLA$_2$ cannot be completely compensated for by other enzymes.

DISCUSSION

Through the use of targeted genetic ablation of iPLA$_2\gamma$, we have demonstrated the fundamental role of this enzyme in cellular bioenergetics that cannot be compensated for by alterations in other enzymic activities. Previously, we hypothesized that iPLA$_2\gamma$ had an important role in modulating cellular bioenergetics based on identification of its mitochondrial localization (8, 29). The findings in this study that iPLA$_2\gamma$ KO mice have attenuated growth, decreased exercise endurance, cold intolerance, and the inability to compensate for increased cardiac stress after hemodynamic overload collectively provide strong evidence of mitochondrial dysfunction induced by iPLA$_2\gamma$ deficiency. The biochemical mechanisms leading to mitochondrial dysfunction were localized to defects in Complex IV function demonstrated by the inability to increase O_2 reduction provoked by ascorbate. In addition, lipidomics analyses indicated that the dysfunction was probably related to alterations in the content of tetra-18:2 cardiolipin molecular species. It has been demonstrated previously by multiple techniques, including co-crystallization and blue native gel electrophoresis, that CL is tightly associated with Complex IV (39–42). Moreover, the CL molecular species specifically associated with cytochrome oxidase is symmetric tetra-18:2 CL, which occupies a tightly associated and highly symmetric position in the complex (43). The absence of iPLA$_2\gamma$ in murine myocardium probably results in a paucity of CL lysocardiolipin acceptor, which limits CL remodeling and the resultant synthesis of tetra-18:2 CL (Fig. 9) (44). The deficiency of tetra-18:2 CL was anticipated based upon the known importance of phospholipases in the remodeling of newly synthesized CL molecular species. This deficiency in symmetric CL molecular species probably results in inefficient Complex IV function, as demonstrated by mitochondrial function assays *in vitro*. The inability of mitochondria to adapt effectively to a variety of stressors under pathophysiologic conditions underscores the importance of specific CL molecular species in mitochondrial bioenergetic efficiency and the important role of iPLA$_2\gamma$ in generating the lysocardiolipin acceptor necessary for the generation of symmetric tetra-18:2 CL molecular species. We specifically point out that other alterations, in addition to the changes in CL content and molecular species composition, could contribute to the dysfunctional mitochondrial adaptations to stress that were demonstrated in this study, including cryptic changes in lipid-protein interactions, alterations in membrane dynamics, and changes in membrane surface charge and distribution.

The iPLA$_2\gamma$ KO phenotype is consistent with an extensive literature demonstrating the association between mitochondrial dysfunction and deficiencies in growth as well as cold and exercise tolerance (3,45–48). Previously, it has been demonstrated in many models that mitochondrial integrity is essential for cold adaptation (38,49–52). Thus, the ability to adapt to cold has previously been utilized to identify mitochondrial dysfunction in many different types of mice with genetic alterations in energy-producing pathways (*e.g.* MCAD (53), UCP1 (54), GPAT1 (55), orphan nuclear receptor estrogen (56), and PGC-1γ (57,58)). Mutations in mitochondrial proteins encoded by both mitochondrial DNA and nuclear DNA have been implicated in a wide range of degenerative diseases, which include clinical features of myopathy, cardiomyopathy, growth retardation, movement disorders, and diabetes. Many animal models have confirmed that alterations in mitochondrial energy generation, ROS production, and apoptosis can all contribute to the pathophysiology of mitochondrial dysfunction (59–62).

Recent investigations into the role of mitochondrial membrane dynamics have uncovered the critical role of mitochondrial membrane fusion and fission in facilitating mitochondrial function (63–65). Although the precise mechanisms that mediate fusion and fission are not known with certainty, it is clear that CL, which has a propensity for HII phase formation, plays a critical role in this process (66). The large difference in the volume occupied by the four highly unsaturated aliphatic chains of CL compared with that of the polar head groups probably promotes prominent curvature of the inner membrane (67). In addition, the doubly anionic charge present in CLs has profound effects on membrane surface charge and facilitates specific lipid-protein interactions. Although the structural features of polyunsaturated CLs have yet to be assigned specific mechanistic roles, the unique characteristics of this molecule and its highly symmetric configuration are probably critical to mitochondrial function on many levels. The production of symmetric CL species is facilitated by iPLA$_2\gamma$ and, as shown in the genetic knock-out, cannot be compensated for by the other phospholipases present in the mitochondrial compartment.

The iPLA$_2\gamma$ KO mice had significantly reduced cold tolerance, yet there were no large differences in expression of UCP1 under basal conditions or after cold induction. Considering the cold intolerance and lower basal core body temperature of the KO (probably due to mitochondrial inefficiency in heat generation), the small increase in KO UCP1 is not unexpected and may represent a compensatory mechanism for heat generation. Prior work has demonstrated the obligatory role of fatty acids in facilitating the function of uncoupling proteins (68–71). Thus, by providing fatty acids locally, mitochondrial phospholipases could function in the acute regulation of inner membrane UCP activity. The significance of the large down-regulation of UCP3 expression in the myocardium of iPLA$_2\gamma$ KO mice is unknown, as is the precise functional role of UCP3 itself.

Phospholipases could also play a key role in regulating the relative proportion of Gibbs free energy in substrate converted into either chemical energy (*e.g.* ATP) or heat in the mitochondria. In many systems previously studied, the role of phospholipases is to regulate signaling functions. In this regard, we point out that iPLA$_2\gamma$ selectively generates 2-arachidonyl (AA) (20:4) LPC, which serves as a node in lipid second messenger signaling pathways (12, 72,73). Support for the role of iPLA$_2\gamma$ in the generation of 2-AA LPC as well as 2-docosahexaenoyl (2-DHA) (22:6)-LPC *in vivo* has come from transgenic mice overexpressing iPLA$_2\gamma$ in a cardiac restricted manner, where dramatic increases in 2-AA LPC and 2-DHA LPC have been demonstrated (29).

A fourth function of phospholipase activity in mitochondria may be to regulate the binding and dynamics of cytochrome *c* to the inner membrane, which is highly dependent on CL content, inner membrane surface charge, and membrane molecular dynamics (74). Thus, abnormal CL content in conjunction with alterations in the physical properties of the mitochondrial inner membrane could significantly change mitochondrial responses to physiologic and pathophysiologic perturbations. Some of the sequelae of altered CL content have been uncovered in the study of the genetic disease Barth syndrome, where a defect in tafazzin synthesis precludes the production of physiologic amounts of CL mass and molecular species (75–78). Notably, CL remodeling by tafazzin requires the generation of lysocardiolipin for subsequent transacylation/reacylation (44). Through the genetic knock-out of iPLA$_2\gamma$, it appears that physiologic CL remodeling does not occur effectively, precipitating mitochondrial dysfunction. It is intriguing to note that the phenotype of Barth syndrome includes growth retardation and cardiomyopathy (79–81), two features recapitulated in the present study.

Genetic ablation of iPLA$_2\gamma$ results in many readily discernable phenotypic alterations. These stand in sharp contrast to the normal growth and development of cPLA$_2\alpha$ and iPLA$_2\beta$ KO mice in which discernable alterations were either limited to the reproductive system or required

careful manipulations of specialized cells to identify alterations (82–85). Recent studies have demonstrated the close structural similarity and evolutionary relationship between the active sites of the $iPLA_2$ and $cPLA_2$ families of enzymes (86). The results of this study clearly identify the role of $iPLA_2\gamma$ in mitochondrial bioenergetic function and underscore its importance in cellular energy metabolism and homeostasis. Based on the importance of mitochondrial efficiency in energy metabolism, it is likely that the alterations described in the present work represent only the major and most easily identifiable abnormalities apparent after genetic ablation. Future studies will probably uncover additional roles for $iPLA_2\gamma$ in mammalian biology as our understanding of the roles of phospholipases and their contribution to the regulation of mitochondrial function expands. The $iPLA_2\gamma$ KO mouse should provide a valuable model toward this goal.

References

1. Goldenthal MJ, Marin-Garcia J. Mol Cell Biochem 2004;262:1–16. [PubMed: 15532704]
2. Marin-Garcia J, Goldenthal MJ. J Mol Med 2004;82:565–578. [PubMed: 15221079]
3. Vercesi AE, Kowaltowski AJ, Oliveira HC, Castilho RF. Front Biosci 2006;11:2554–2564. [PubMed: 16720333]
4. Garrido C, Galluzzi L, Brunet M, Puig PE, Didelot C, Kroemer G. Cell Death Differ 2006;13:1423–1433. [PubMed: 16676004]
5. Duchen MR. Diabetes 2004;53(Suppl 1):96–102.
6. Kinsey GR, McHowat J, Beckett CS, Schnellmann RG. Am J Physiol 2007;292:F853–F860.
7. Gadd ME, Broekemeier KM, Crouser ED, Kumar J, Graff G, Pfeiffer DR. J Biol Chem 2006;281:6931–6939. [PubMed: 16407316]
8. Mancuso DJ, Jenkins CM, Sims HF, Cohen JM, Yang J, Gross RW. Eur J Biochem 2004;271:4709–4724. [PubMed: 15606758]
9. Williams SD, Gottlieb RA. Biochem J 2002;362:23–32. [PubMed: 11829736]
10. Brustovetsky T, Antonsson B, Jemmerson R, Dubinsky JM, Brustovetsky N. J Neurochem 2005;94:980–994. [PubMed: 16092941]
11. Seleznev K, Zhao C, Zhang XH, Song K, Ma ZA. J Biol Chem 2006;281:22275–22288. [PubMed: 16728389]
12. Yan W, Jenkins CM, Han X, Mancuso DJ, Sims HF, Yang K, Gross RW. J Biol Chem 2005;280:26669–26679. [PubMed: 15908428]
13. Su X, Han X, Mancuso DJ, Abendschein DR, Gross RW. Biochemistry 2005;44:5234–5245. [PubMed: 15794660]
14. Turk J, Ramanadham S. Can J Physiol Pharmacol 2004;82:824–832. [PubMed: 15573142]
15. Ramanadham S, Hsu FF, Zhang S, Jin C, Bohrer A, Song H, Bao S, Ma Z, Turk J. Biochemistry 2004;43:918–930. [PubMed: 14744135]
16. Wang Z, Ramanadham S, Ma ZA, Bao S, Mancuso DJ, Gross RW, Turk J. J Biol Chem 2005;280:6840–6849. [PubMed: 15576376]
17. Huss JM, Kelly DP. J Clin Invest 2005;115:547–555. [PubMed: 15765136]
18. Han X, Abendschein DR, Kelley JG, Gross RW. Biochem J 2000;352:79–89. [PubMed: 11062060]
19. Han X, Gross RW. Mass Spectrom Rev 2005;24:367–412. [PubMed: 15389848]
20. Han X, Yang J, Yang K, Zhao Z, Abendschein DR, Gross RW. Biochemistry 2007;46:6417–6428. [PubMed: 17487985]
21. Mingrone G. Ann N Y Acad Sci 2004;1033:99–107. [PubMed: 15591007]
22. Budnik LT, Mukhopadhyay AK. Biol Reprod 2002;67:935–944. [PubMed: 12193405]
23. Budnik LT. Reprod Biol Endocrinol 2003;1:37–38. [PubMed: 12740030]
24. Haber EP, Ximenes HM, Procopio J, Carvalho CR, Curi R, Carpinelli AR. J Cell Physiol 2003;194:1–12. [PubMed: 12447984]
25. MacDonald MJ, Fahien LA, Brown LJ, Hasan NM, Buss JD, Kendrick MA. Am J Physiol 2005;288:E1–E15.

26. Han X, Yang K, Yang J, Cheng H, Gross RW. J Lipid Res 2006;47:864–879. [PubMed: 16449763]
27. Han X, Gross RW. Expert Rev Proteomics 2005;2:253–264. [PubMed: 15892569]
28. Mancuso DJ, Jenkins CM, Gross RW. J Biol Chem 2000;275:9937–9945. [PubMed: 10744668]
29. Mancuso DJ, Han X, Jenkins CM, Lehman JJ, Sambandam N, Sims HF, Yang J, Yan W, Yang K, Green K, Abendschein DR, Saffitz JE, Gross RW. J Biol Chem 2007;282:9216–9227. [PubMed: 17213206]
30. Han X, Cheng H, Mancuso DJ, Gross RW. Biochemistry 2004;43:15584–15594. [PubMed: 15581371]
31. Tybulewicz VL, Crawford CE, Jackson PK, Bronson RT, Mulligan RC. Cell 1991;65:1153–1163. [PubMed: 2065352]
32. Leone TC, Lehman JJ, Finck BN, Schaeffer PJ, Wende AR, Boudina S, Courtois M, Wozniak DF, Sambandam N, Bernal-Mizrachi C, Chen Z, Holloszy JO, Medeiros DM, Schmidt RE, Saffitz JE, Abel ED, Semenkovich CF, Kelly DP. PLoS Biol 2005;3:e101. [PubMed: 15760270]
33. Rockman HA, Ross RS, Harris AN, Knowlton KU, Steinhelper ME, Field LJ, Ross J Jr, Chien KR. Proc Natl Acad Sci U S A 1991;88:8277–8281. [PubMed: 1832775]
34. Xing H, Zhang S, Weinheimer C, Kovacs A, Muslin AJ. EMBO J 2000;19:349–358. [PubMed: 10654934]
35. Ricci JE, Gottlieb RA, Green DR. J Cell Biol 2003;160:65–75. [PubMed: 12515825]
36. Nicholls, DG.; Ferguson, SJ. Bioenergetics. Vol. 3. Academic Press, Inc; London: 2001.
37. Stewart A, Ghosh M, Spencer DM, Leslie CC. J Biol Chem 2002;277:29526–29536. [PubMed: 12039969]
38. Mozo J, Emre Y, Bouillaud F, Ricquier D, Criscuolo F. Biosci Rep 2005;25:227–249. [PubMed: 16283555]
39. Robinson NC. J Bioenerg Biomembr 1993;25:153–163. [PubMed: 8389748]
40. Gomez B Jr, Robinson NC. Biochemistry 1999;38:9031–9038. [PubMed: 10413476]
41. Zhang M, Mileykovskaya E, Dowhan W. J Biol Chem 2002;277:43553–43556. [PubMed: 12364341]
42. Tsukihara T, Shimokata K, Katayama Y, Shimada H, Muramoto K, Aoyama H, Mochizuki M, Shinzawa-Itoh K, Yamashita E, Yao M, Ishimura Y, Yoshikawa S. Proc Natl Acad Sci U S A 2003;100:15304–15309. [PubMed: 14673090]
43. Shinzawa-Itoh K, Aoyama H, Muramoto K, Terada H, Kurauchi T, Tadehara Y, Yamasaki A, Sugimura T, Kurono S, Tsujimoto K, Mizushima T, Yamashita E, Tsukihara T, Yoshikawa S. EMBO J 2007;26:1713–1725. [PubMed: 17332748]
44. Xu Y, Malhotra A, Ren M, Schlame M. J Biol Chem 2006;281:39217–39224. [PubMed: 17082194]
45. Filosto M, Mancuso M. Acta Neurol Scand 2007;115:211–221. [PubMed: 17376118]
46. Ritz P, Dumas JF, Ducluzeau PH, Simard G. Curr Opin Clin Nutr Metab Care 2005;8:415–418. [PubMed: 15930967]
47. Siciliano G, Volpi L, Piazza S, Ricci G, Mancuso M, Murri L. Biosci Rep 2007;27:53–67. [PubMed: 17492503]
48. McFarland R, Taylor RW, Turnbull DM. Curr Top Dev Biol 2007;77:113–155. [PubMed: 17222702]
49. Ricquier D. Proc Nutr Soc 2005;64:47–52. [PubMed: 15877922]
50. Silva JE. Physiol Rev 2006;86:435–464. [PubMed: 16601266]
51. Klingenspor M. Exp Physiol 2003;88:141–148. [PubMed: 12525862]
52. Nedergaard J, Golozoubova V, Matthias A, Shabalina I, Ohba K, Ohlson K, Jacobsson A, Cannon B. Biochem Soc Trans 2001;29:756–763. [PubMed: 11709070]
53. Tolwani RJ, Hamm DA, Tian L, Sharer JD, Vockley J, Rinaldo P, Matern D, Schoeb TR, Wood PA. PLoS Genet 2005;1:e23. [PubMed: 16121256]
54. Monemdjou S, Hofmann WE, Kozak LP, Harper ME. Am J Physiol 2000;279:E941–E946.
55. Gonzalez-Baro MR, Lewin TM, Coleman RA. Am J Physiol 2007;292:G1195–G1199.
56. Villena JA, Hock MB, Chang WY, Barcas JE, Giguere V, Kralli A. Proc Natl Acad Sci U S A 2007;104:1418–1423. [PubMed: 17229846]
57. Sonoda J, Mehl IR, Chong LW, Nofsinger RR, Evans RM. Proc Natl Acad Sci U S A 2007;104:5223–5228. [PubMed: 17360356]

58. Lelliott CJ, Medina-Gomez G, Petrovic N, Kis A, Feldmann HM, Bjursell M, Parker N, Curtis K, Campbell M, Hu P, Zhang D, Litwin SE, Zaha VG, Fountain KT, Boudina S, Jimenez-Linan M, Blount M, Lopez M, Meirhaeghe A, Bohlooly YM, Storlien L, Stromstedt M, Snaith M, Oresic M, Abel ED, Cannon B, Vidal-Puig A. PLoS Biol 2006;4:e369. [PubMed: 17090215]
59. Wallace DC. Methods Mol Biol 2002;197:3–54. [PubMed: 12013805]
60. Wallace DC. Am J Med Genet 2001;106:71–93. [PubMed: 11579427]
61. Wallace DC. Annu Rev Genet 2005;39:359–407. [PubMed: 16285865]
62. Wallace DC. Ment Retard Dev Disabil Res Rev 2001;7:158–166. [PubMed: 11553931]
63. Chen JL, Peacock E, Samady W, Turner SM, Neese RA, Hellerstein MK, Murphy EJ. J Biol Chem 2005;280:25396–25402. [PubMed: 15888453]
64. Heath-Engel HM, Shore GC. Biochim Biophys Acta 2006;1763:549–560. [PubMed: 16574258]
65. McBride HM, Neuspiel M, Wasiak S. Curr Biol 2006;16:R551–560. [PubMed: 16860735]
66. Siegel DP. Biophys J 1984;45:399–420. [PubMed: 6365189]
67. Dahlberg M. J Phys Chem B 2007;111:7194–7200. [PubMed: 17542632]
68. Skulachev VP. FEBS Lett 1991;294:158–162. [PubMed: 1756853]
69. Garlid KD, Orosz DE, Modriansky M, Vassanelli S, Jezek P. J Biol Chem 1996;271:2615–2620. [PubMed: 8576230]
70. Breen EP, Gouin SG, Murphy AF, Haines LR, Jackson AM, Pearson TW, Murphy PV, Porter RK. J Biol Chem 2006;281:2114–2119. [PubMed: 16291746]
71. Porter RK. Biochim Biophys Acta 2006;1757:446–448. [PubMed: 16730638]
72. Di Marzo V, De Petrocellis L, Sugiura T, Waku K. Biochem Biophys Res Commun 1996;227:281–288. [PubMed: 8858137]
73. Pete MJ, Exton JH. J Biol Chem 1996;271:18114–18121. [PubMed: 8663471]
74. Pinheiro TJ, Watts A. Biochemistry 1994;33:2459–2467. [PubMed: 8117706]
75. Vreken P, Valianpour F, Nijtmans LG, Grivell LA, Plecko B, Wanders RJ, Barth PG. Biochem Biophys Res Commun 2000;279:378–382. [PubMed: 11118295]
76. Schlame M, Towbin JA, Heerdt PM, Jehle R, DiMauro S, Blanck TJ. Ann Neurol 2002;51:634–637. [PubMed: 12112112]
77. Xu Y, Kelley RI, Blanck TJ, Schlame M. J Biol Chem 2003;278:51380–51385. [PubMed: 14551214]
78. Schlame M, Ren M, Xu Y, Greenberg ML, Haller I. Chem Phys Lipids 2005;138:38–49. [PubMed: 16226238]
79. Spencer CT, Bryant RM, Day J, Gonzalez IL, Colan SD, Thompson WR, Berthy J, Redfearn SP, Byrne BJ. Pediatrics 2006;118:e337–346. [PubMed: 16847078]
80. Bolhuis PA, Hensels GW, Hulsebos TJ, Baas F, Barth PG. Am J Hum Genet 1991;48:481–485. [PubMed: 1998334]
81. Schlame M, Ren M. FEBS Lett 2006;580:5450–5455. [PubMed: 16973164]
82. Bonventre JV, Huang Z, Taheri MR, O'Leary E, Li E, Moskowitz MA, Sapirstein A. Nature 1997;390:622–625. [PubMed: 9403693]
83. Fujishima H, Sanchez Mejia RO, Bingham CO III, Lam BK, Sapirstein A, Bonventre JV, Austen KF, Arm JP. Proc Natl Acad Sci U S A 1999;96:4803–4807. [PubMed: 10220374]
84. Rosenberger TA, Villacreses NE, Contreras MA, Bonventre JV, Rapoport SI. J Lipid Res 2003;44:109–117. [PubMed: 12518029]
85. Bao S, Miller DJ, Ma Z, Wohltmann M, Eng G, Ramanadham S, Moley K, Turk J. J Biol Chem 2004;279:38194–38200. [PubMed: 15252026]
86. Wilson PA, Gardner SD, Lambie NM, Commans SA, Crowther DJ. J Lipid Res 2006;47:1940–1949. [PubMed: 16799181]

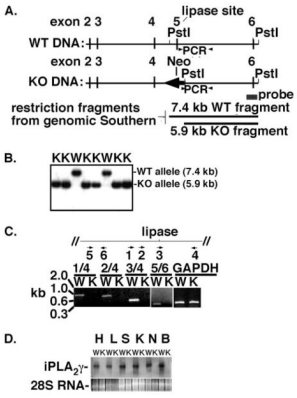

FIGURE 1. Strategy for iPLA$_2\gamma$ gene ablation and genetic and expression analyses

A, schematic representation of the iPLA$_2\gamma$ gene-targeting strategy. The region of the wild type murine iPLA$_2\gamma$ gene containing exons 2– 6 is shown schematically (*top*) along with the predicted knock-out region resulting from homologous recombination (*below*). Relevant restriction endonuclease sites are also shown. The neomycin cassette is indicated by a *shaded arrow* (labeled *Neo*). The regions between exons 3 and 4 and between exons 5 and 6 were targeted for homologous recombination. The locations of PCR primers utilized for tail PCR genetic analyses are indicated with *arrows* (labeled *PCR*). The region corresponding to the probe used for genomic Southern blot analyses is indicated as a *shaded box* (labeled *probe*), whereas relevant restriction fragments resulting from PstI restriction digestion of the WT and KO are indicated. *B*, genomic Southern analysis of wild type and iPLA$_2\gamma$ knock-out mice. Southern blot analyses of genomic DNA from wild type and iPLA$_2\gamma$ null mice were performed utilizing tail DNA digested with PstI and hybridized with the probe indicated in Fig. 1*A*. Autoradiography of the genomic Southern blots revealed the presence of an expected 7.4-kb wild type allelic band labeled as *W* in *lanes 3* and *6*, whereas analyses of iPLA$_2\gamma$ knockouts labeled as *K* in *lanes 1*, *2*, *4*, *5*, *7*, and *8* revealed the presence of the predicted 5.9-kb knock-out allele band. Results are representative of separate Southern analyses of genomic DNA from over 30 animals. *C*, PCR analyses of different regions of the iPLA$_2\gamma$ coding sequence. Primers 1– 6 (represented by *arrows below* the *schematic* of the iPLA$_2\gamma$ coding sequence (*top*) surrounding the lipase active site) were paired as indicated (5′-primer/3′-primer *underlined*) to amplify by PCR different regions of the sequence utilizing cDNA prepared from either WT or KO heart RNA as template. Agarose-gel electrophoresis demonstrated the presence of amplified PCR products of the expected size (in kb) utilizing only wild type (*W*) and not knock-out (*K*) template with primer pairs 1/4, 2/4, 3/4, and 5/6. PCR products amplified from both wild type and knock-out template utilizing a control GAPDH primer pair are shown at the *right*. Data are representative of those obtained from reverse transcription-PCR analyses of RNA from the myocardium of three separate animals. *D*, expression of iPLA$_2\gamma$ mRNA in wild type but not iPLA$_2\gamma$ knock-out tissues. Total RNA was isolated from heart (*H*), liver (*L*), skeletal (*S*), kidney (*K*), lung (*N*), and brain (*B*) tissues wild type (*W*) and iPLA$_2\gamma$ knock-out (*K*) prior to separation by agarose-gel electrophoresis and Northern blot analysis using a 1-kb probe complementary to the region of iPLA$_2\gamma$ cDNA (*iPLA$_2\gamma$*) flanking the sequence encoding the lipase site. Ethidium bromide staining of 28 S ribosomal RNA (*28S RNA*) in each corresponding *lane* is shown *below*. Results are representative of separate Northern analyses of RNA extracted from multiple tissues from three WT and three KO animals.

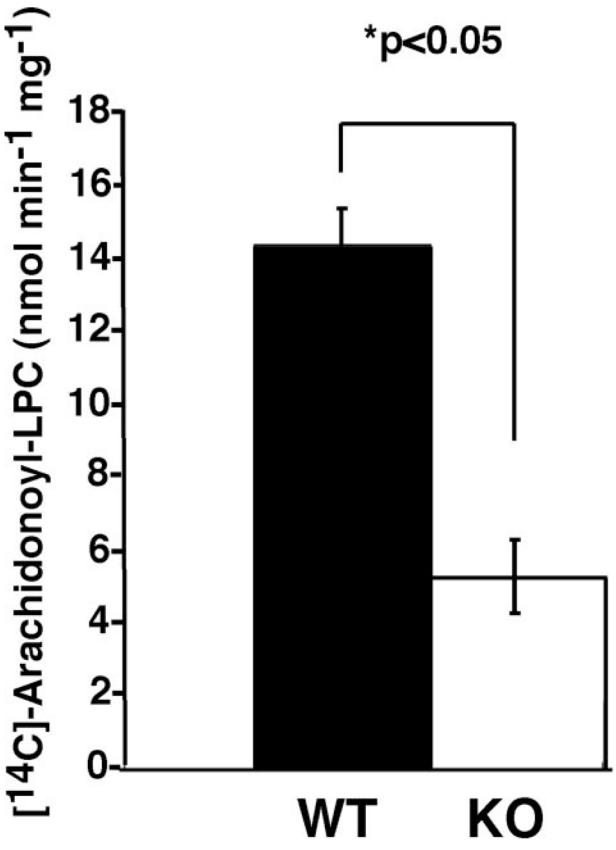

FIGURE 2. iPLA$_2\gamma$ activity in wild type and iPLA$_2\gamma$ knock-out mouse myocardial mitochondria

Calcium-independent phospholipase A$_2\gamma$ has been previously demonstrated to selectively hydrolyze 1-palmitoyl-2-[1-^{14}C]arachidonoyl phosphatidylcholine to generate 2-[1-^{14}C] arachidonoyl LPC (12). To selectively measure iPLA$_2\gamma$ activity among other cellular mitochondrial phospholipases, mitochondria were isolated from WT and KO hearts, sonicated, and incubated in the presence of 1-palmitoyl-2-[1-^{14}C]arachidonoyl phosphatidylcholine as described under "Experimental Procedures." Remaining radiolabeled substrate and reaction products were extracted into butanol and resolved by TLC, and the amount of 2-[^{14}C] arachidonoyl LPC was determined by scintillation spectrometry counting and expressed as nmol of 2-[^{14}C]arachidonoyl LPC min^{-1} mg of mitochondrial protein^{-1}. A dramatic 60% reduction in the production of 2-arachidonoyl LPC was observed in KO mitochondria in comparison with their WT counterparts (*, $p < 0.05$). All data were averaged from analyses of duplicate determinations from three mice and are shown as mean ± S.D.

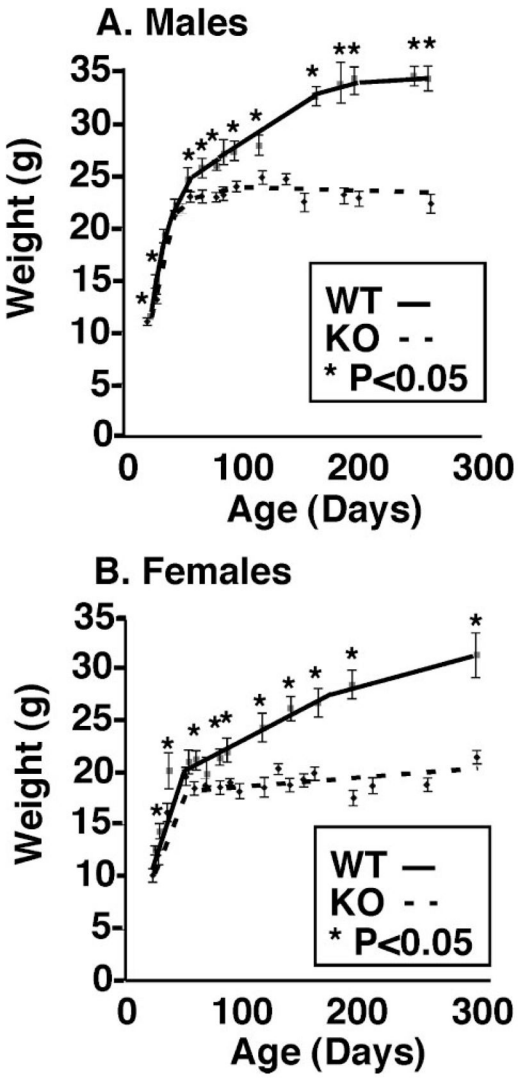

FIGURE 3. Severely reduced growth rate of iPLA$_2\gamma$ KO mice in comparison with WT controls

Total average body weight (g) was measured and plotted *versus* age (in days) for male (*A*) and female (*B*) WT and iPLA$_2\gamma$ KO mice. The results represent 155 measurements of 43 wild type and 33 knock-out males and 25 wild type and 33 knock-out females between the ages of 28 and 282 days. Values represent the mean ± S.E. for each data point. Both male and female iPLA$_2\gamma$ KO animals (*dashed lines*) had significantly decreased growth (*, $p < 0.05$) as early as day 28 (by Student's *t* test) in comparison with WT littermates (*solid lines*). KO animals demonstrated severe growth retardation after approximately day 50 with very little weight gain through day 280.

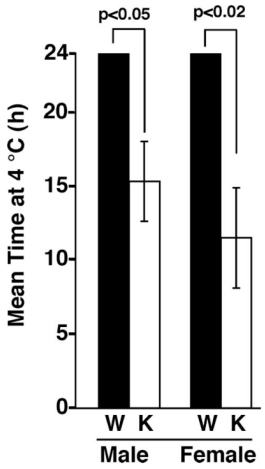

FIGURE 4. Cold intolerance of iPLA$_{2\gamma}$ KO mice

For cold tolerance tests, mice (4 – 6 months) were individually housed at 4°C in standard breeding cages containing bedding with free access to food and water. Rectal core body temperatures were measured using a thermocouple probe inserted 2 cm into the rectum until a stable reading was obtained. Measurements were taken every 60 min for up to 24 h or until the mice became torpid or the core temperature dropped below ~28°C, after which mice were removed for recovery. All WT mice maintained their body temperature between 30 and 36°C during the entire course of the studies (24 h). The *bar graph* shows mean cold tolerance time ± S.E. for male and female WT (*solid bars*) and KO (*open bars*) animals. The mean time at which male KO mice were able to maintain their core body temperature was 15.3 ± 2.7 h (n = 6 per group, $p < 0.05$ by Student's t test) compared with WT controls (which maintained their body temperatures for the entire experimental interval). For female KOs, the corresponding mean endurance time at 4°C was 11.5 ± 3.4 h (n = 6 per group, $p < 0.02$) compared with WT controls, which maintained their body temperatures throughout the entire experimental interval.

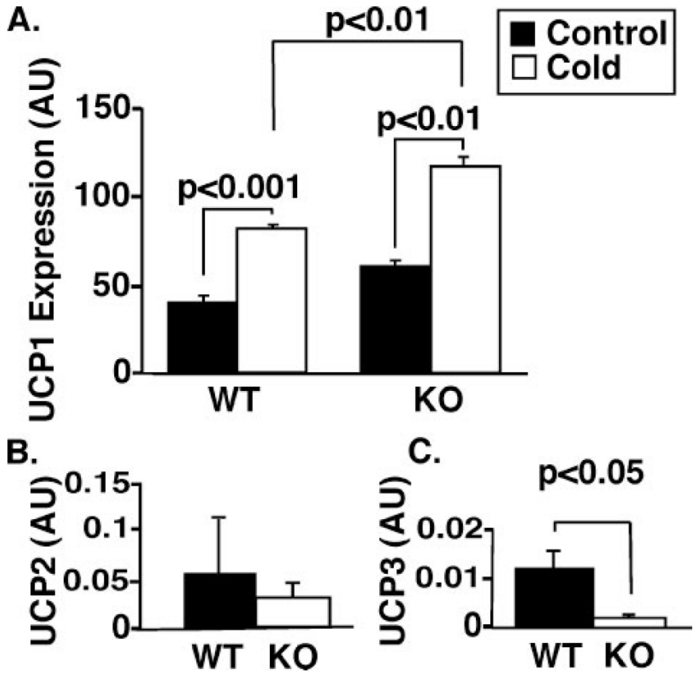

FIGURE 5. Expression of UCP1 mRNA in brown adipose tissue and also UCP2 and UCP3 mRNA in heart tissue from WT and KO mice

Expression levels of UCP1 (*A*), UCP2 (*B*), and UCP3 (*C*) mRNA were measured using real time PCR as described under "Experimental Procedures." *A*, UCP1 message levels in brown adipose tissue were measured under ambient conditions (control) and during exposure to cold (4°C). Animals were exposed to 4°C until their core body temperature dropped to hypothermic levels (below ~28°C). The mean cold tolerance time for KO animals was 8 h, and WT controls (still maintaining the core body temperatures) were sacrificed at the same mean time. *B*, no significant difference was observed for UCP2 expression levels in WT and KO hearts. *C*, a significant reduction in UCP3 expression was observed in the hearts of iPLA$_2\gamma$ KO mice ($p < 0.05$). $n = 4$ per group. Values represent arbitrary units (*AU*) after normalization to a ribosomal 36B4 internal standard. Data are presented as means ± S.E. Statistical significance was performed using the Student's *t* test, and significant differences are indicated by *brackets*.

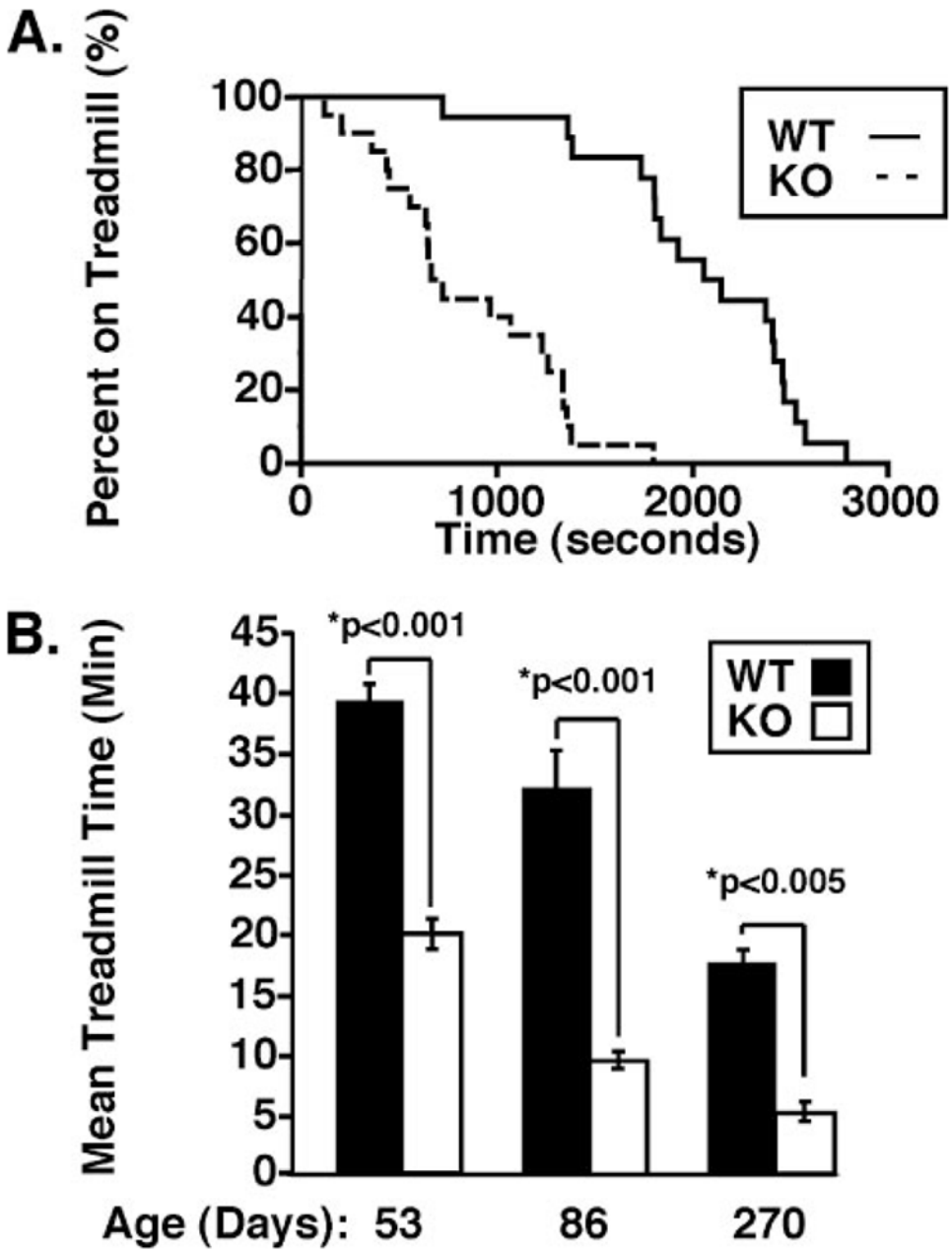

FIGURE 6. Reduced exercise capacity of the iPLA$_2\gamma$ knock-out

A, Kaplan-Meier survival curve analysis of iPLA$_2\gamma$ KO and WT treadmill performance plotted as the percentage of animals remaining on the treadmill *versus* time (s). iPLA$_2\gamma$ WT (n = 20) and iPLA$_2\gamma$ KO (n = 22) male and female mice aged 2–4 months were subjected to an exercise-to-exhaustion protocol on a motorized treadmill, as described under "Experimental Procedures." Median exercise times were 2103 and 692 s for WT and KO animals, respectively, $p < 0.001$ by one-way analysis of variance. *B*, a significant reduction in exercise endurance was revealed for mice null for iPLA$_2\gamma$ when the above data were replotted as treadmill time *versus* mean age in days comparing mice of ~53, 86, and 270 days. Treadmill times for iPLA$_2\gamma$ KO mice were approximately half those for WT animals at 53 days but dropped to nearly 25% of WT treadmill times by day 86. *, $p < 0.001$ by Student's t test.

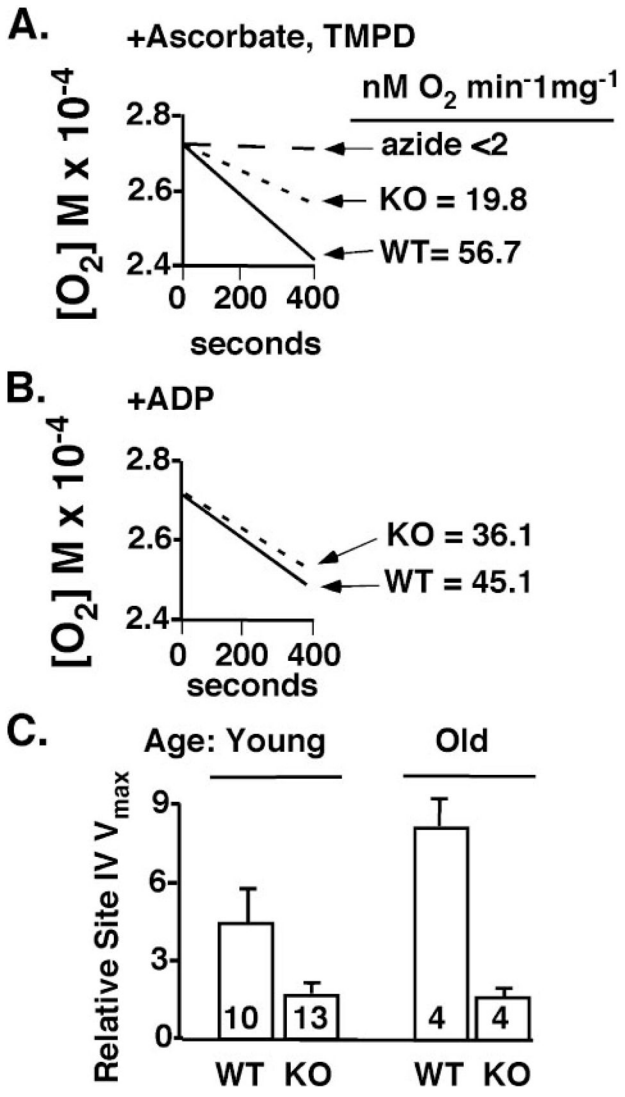

FIGURE 7. Functional analysis of wild type and knock-out iPLA$_{2}\gamma$ isolated myocardial mitochondria

Mitochondria were isolated, and oxygen consumption was measured under different experimental conditions as described under "Experimental Procedures." *A*, a representative TMPD-ascorbate-supported oxygen consumption by mitochondria from WT and KO animals is shown. The calculated rates of oxygen consumption were normalized for protein concentration. Also shown is the effect of azide upon the TMPD-ascorbate oxygen consumption. *B*, a representative graph of the malate-ADP-supported oxygen consumption by mitochondria from WT and KO animals. The calculated rates of oxygen consumption are normalized for protein concentration. *C*, ascorbate-TMPD oxygen consumption (plotted as relative site IV V_{max}) is corrected for azide inhibition and summarized for all animals in WT and KO groups. $n = 6$ young (4 – 6 months) and 3 old (9 –11 months) animals/group. The *numbers within* each *bar* indicate the total number of mitochondrial measurements. Analyses of these results indicate that for both age groups, the KO reduces the observed azide-inhibitable oxygen consumption ($p < 0.05$).

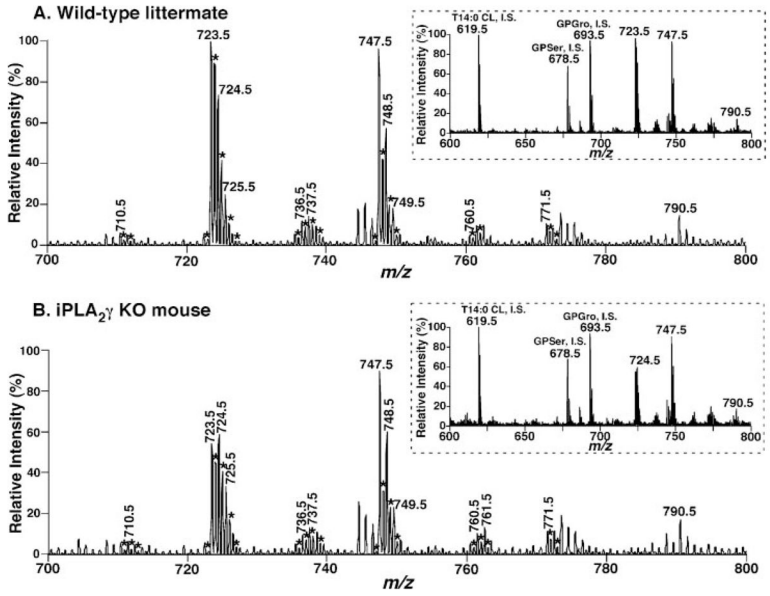

FIGURE 8. Expanded negative ion electrospray ionization mass spectra of myocardial lipid extracts from iPLA$_{2}\gamma$ KO mice and their wild type littermates

Myocardial lipid extracts of wild type mice (*A*) and iPLA$_{2}\gamma$ KO mice (*B*) were prepared by a modified Bligh and Dyer procedure. Negative ion electrospray ionization mass spectra were acquired using a QqQ mass spectrometer as described under "Experimental Procedures." Spectra have been normalized to a CL internal standard (see *insets*). The *asterisks* indicate the doubly charged CL plus-one isotopologues whose ion peak intensities were utilized to quantify individual CL molecular species as described previously (26). The results indicate the paucity of tetra-18:2 CL molecular species in the iPLA$_{2}\gamma$ KO in comparison with WT (compare peaks at *m*/*z* 723.5 in control *versus* iPLA$_{2}\gamma$ KO). The *insets* on the *right* of each *panel* show the extended mass spectra that display additional internal standards and other major anionic phospholipids.

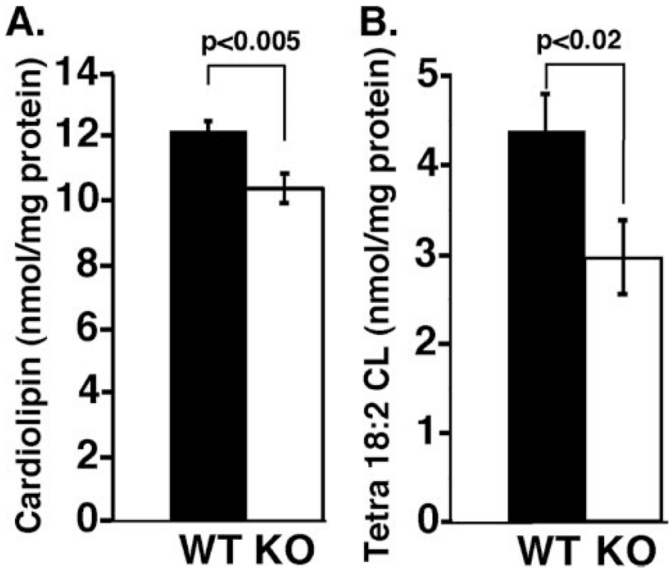

FIGURE 9. Cardiolipin content of iPLA$_{2}\gamma$ knock-out mouse myocardium

Mouse heart tissues were obtained from 3–4-month-old wild type (*WT*) or iPLA$_{2}\gamma$ KO (*KO*) mice fed *ad libitum*. Mouse myocardial lipids were extracted by a modified Bligh and Dyer method and subjected to electrospray ionization/mass spectrometry analyses in the negative ion mode as described under "Experimental Procedures." The levels of individual cardiolipin molecular species after identification were calculated in comparison with the selected internal standard after ^{13}C deisotoping as described previously (26). *A*, alterations in total cardiolipin content (nmol of CL/mg of protein) between WT and iPLA$_{2}\gamma$ KO mice. *B*, alterations in the content of the major cardiolipin species, tetra-18:2 CL (nmol/mg protein) in iPLA$_{2}\gamma$ KO *versus* WT mice. Experiments were performed with three WT and five KO animals between 3 and 6 months in age. Significant decreases in both total cardiolipin ($p < 0.005$) and tetra-18:2 CL species ($p < 0.02$) were consistently observed in iPLA$_{2}\gamma$ KO hearts.

TABLE 1
Primers for construction and genotyping of the iPLA$_2\gamma$ knock-out

iPLA$_2\gamma$ KO primers P1–P4 were used in PCR to prepare the KO construct. PCR primers P5 and P6 were used to generate the 459-nt genomic probe for genotyping by genomic Southern blot analyses. The tail PCR primer set was used for genotyping. “Neo forward” paired with the “Common REV” amplified a 354-nt product from KO DNA whereas “iPLA$_2\gamma$ FOR” paired with “Common REV” amplified a 181-nt product from WT DNA. Reverse transcription-PCR primers 1–6 were used to demonstrate an absence of iPLA$_2\gamma$ message expression from the KO, whereas “GAPDH F” and “GAPDH R” PCR primers were used as positive controls for amplification of GAPDH PCR product from both WT and KO cDNA.

Primers	Sequence (5′–3′)
iPLA$_2\gamma$ KO primers	
P1	AAAAGAATTCAGGCAGAGGAGAAAAAGCGTGTGCTACTTC
P2	AAAAGAATTCGCTCACAACCATCCGTAATGAGATCTGGATG
P3	AAAACTCGAGCCAAGAACATGCAGCACAGGCTTGAGGCCAT
P4	AAAAGCGGCCGCTTGTTGACATCATAAAAACCATAATT
P5	CTCTATCGAAAGTTGGGCTCAGATGT
P6	AATAGGTAAATAAATACTAAAATGGA
Tail PCR primer set	
NEO forward	AAAGGCCTACCCGCTTCCATTGCTCA
Common REV	GCCTCAAGCCTGTGCTGCATGTTCTT
iPLA$_2\gamma$ FOR	CTGTTCACAGAGGTGTGGTTGC
KO band = 354 base pairs	
WT band = 181 base pairs	
Reverse transcription-PCR primers	
1	CAAGAAGGCAGAGGAGAAAAAGC
2	CCCAAAGCTCTGTATTACTAGGG
3	GATTACATCTGTGGAGTAAGCACAGGG
4	CGTGAAAGGCCAAGGCCGAAGGG
5	AGTGAGCATTCATATGTCCCG
6	CGGAGAATGACTCTCCAAATCTG
GAPDH F	TGTTGCCATCAATGACCCCTTCA
GAPDH R	TGATGATCTTGAGGCTGTTGTC